[DC-03-031] Hyperspectral Remote Sensing

Abstract

Hyperspectral remote sensing (HRS) is a specialized technique that collects and processes hundreds of contiguous spectral bands across a broad range of electromagnetic wavelengths. Unlike multispectral remote sensing, which records only a few discrete broad bands (e.g., 30 nm) HRS acquires continuous spectra in narrow bandwidths (e.g., 5 nm). This capability provides a richer set of spectral signatures, enabling more precise identification of surface materials, vegetation, and minerals, among other applications. Although HRS applies many of the same physical principles as multispectral remote sensing, it requires specialized instruments, data collection procedures, and analytical methods.

Author & citation

Qi, Y. (2025). Hyperspectral Remote Sensing. The Geographic Information Science & Technology Body of Knowledge (Issue 1, 2025 Edition), John P. Wilson (ed.), DOI: 10.22224/gistbok/2025.1.16

Explanation

1. Hyperspectral Remote Sensing (HRS) Defined

Hyperspectral remote sensing (HRS) is a specialized technique that collects and processes hundreds of contiguous spectral bands across a broad range of electromagnetic wavelengths. Unlike multispectral remote sensing, which records only a few discrete broad bands (e.g., 30 nm), HRS acquires continuous spectra in narrow bandwidths (e.g., 5 nm). This capability provides a richer set of spectral signatures, enabling more precise identification of surface materials, vegetation, and minerals, among other applications (Figure 1). Although HRS applies many of the same physical principles as multispectral remote sensing, it requires specialized instruments, data collection procedures, and analytical methods.

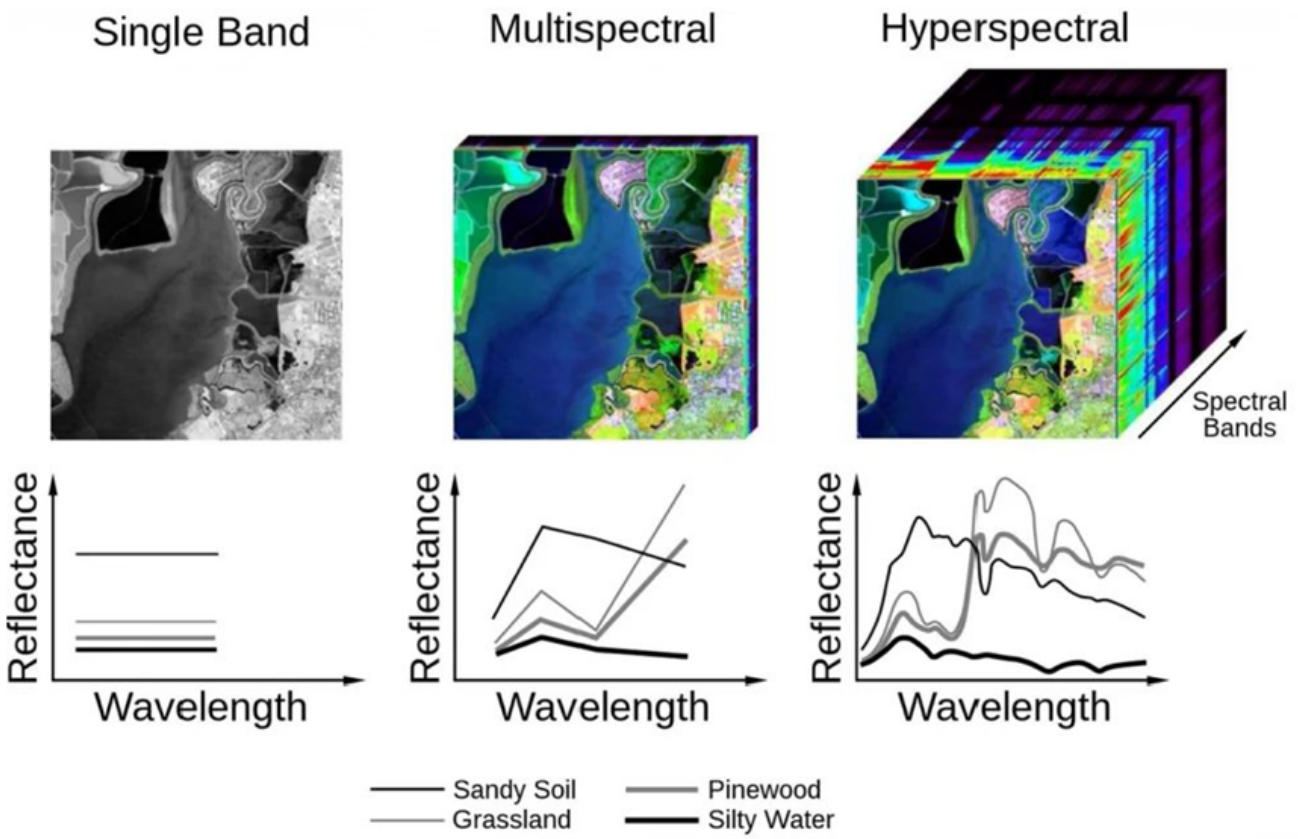

Figure 1. The illustrated concept of HRS in comparison with single band and multispectral remote sensing. The continuous spectra of HRS across hundreds of narrow bands between 400 and 2500 nm wavelengths provide more detailed spectroscopic information in the object of interests. Source: Innoter.com.

Hyperspectral remote sensing (HRS) originated from the principles of spectroscopy, which examines how matter interacts with electromagnetic radiation across a range of wavelengths. HRS encompasses both non-imaging spectroscopy (Curran, 1989)—typically conducted in laboratory or close-range settings to measure small samples—and imaging spectroscopy (Goetz et al., 2009), which acquires hyperspectral images of larger landscapes or objects. A variety of HRS instruments capture spectral information across the visible, near-infrared, shortwave infrared, mid-wave infrared, and thermal infrared regions. Among the most commonly used systems are passive remote sensing devices designed to measure reflectance within solar wavelengths (0.4–2.5 µm). The discussion here focuses on this specific HRS system.

2. Physical Foundation of HRS: Spectroscopy

Spectroscopy is the study of how electromagnetic radiation interacts with matter as a function of wavelength. Depending on the type of interaction and the wavelengths examined, the field includes sub-disciplines focusing on absorption, emission, reflectance, and fluorescence. The core principle of spectroscopy is that each material interacts with electromagnetic radiation in a unique way at different wavelengths, producing a characteristic spectral signature that reveals its composition, structure, and physical properties (Kokaly et al., 2009). This versatility has led to broad applications of spectroscopy in physics, chemistry, environmental science, and the food industry.

Spectroscopy provides the fundamental physical basis of HRS by linking the electromagnetic spectrum to the vibrational and electronic resonances of molecules, as well as to microscopic surface and volumetric properties. In HRS that measures solar-reflective spectra, most natural materials exhibit diagnostic absorption features primarily driven by two spectroscopic processes at different wavelengths. First, in the visible to near-infrared ranges, electronic transitions and charge transfer processes—often influenced by transition metal ions such as Fe, Ti, Cr, Co, and Ni—determine the positions of characteristic absorption features. Second, in the shortwave and mid-infrared regions, vibrational processes involving water (H_2O) and hydroxyl (OH^-), as well as carbonate and sulfate groups, govern the absorption features (Figure 2). These diagnostic absorptions alter the reflectance spectrum recorded by HRS, thereby revealing the chemical composition and physical properties of the target materials.

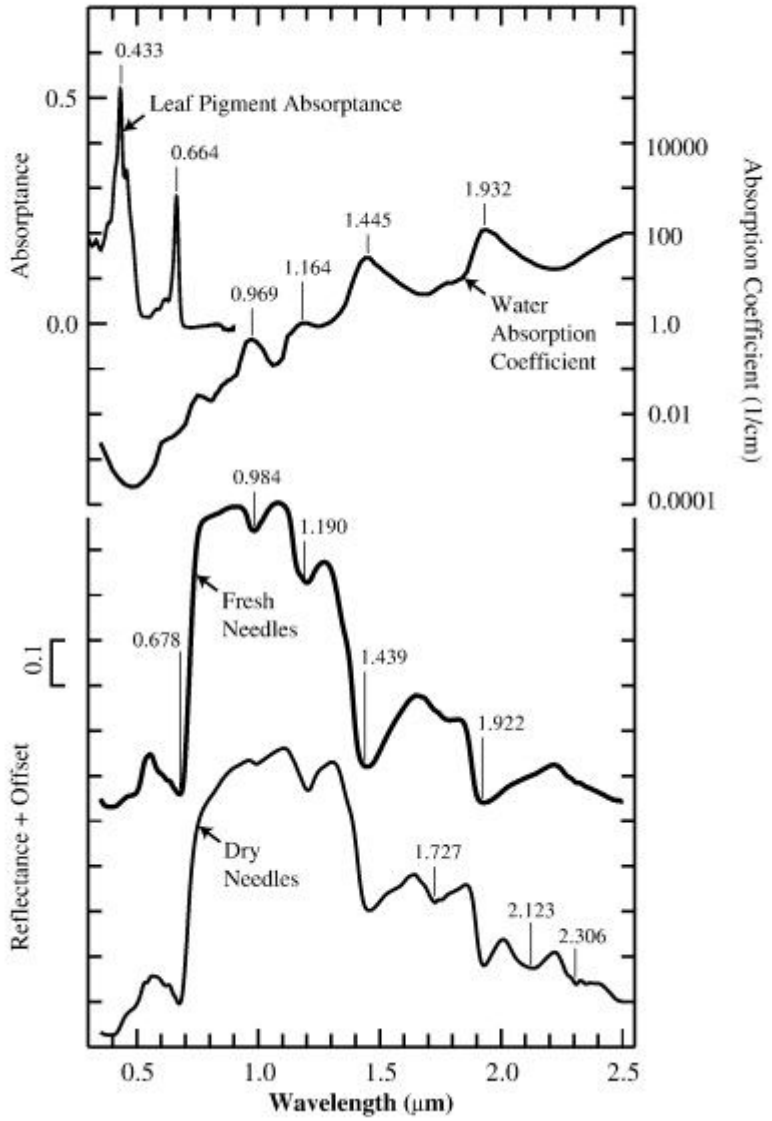

Figure 2. Reflectance spectra of stacked lodgepole pine needles measured in the laboratory in fresh (thick line) and dry (thin line) states. The absorptance spectrum of extracted leaf pigments and the water absorption coefficient (on a log scale) are shown as references. The wavelength positions of strong absorption features are given. The reflectance levels at 0.8 μm are 0.55 and 0.67 for the spectra of dry needles and fresh needles, respectively. Source: Kokaly et al., 2029; used with permission.

3. Non-imaging HRS: Field Spectroscopy

Field spectroscopy (non-imaging hyperspectral remote sensing) involves measuring the reflectance spectra of objects in laboratories or close-range environments (Milton et al., 2009). It emerged in the 1970s with the development of field spectrometers designed to capture accurate spectral reflectance data under field conditions. Today, various portable spectrometers from different manufacturers operate at different spectral ranges and resolutions. For instance, the ASD FieldSpec 4 Hi-Res Spectrometer (Malvern Panalytical) records wavelengths between 350 and 2500 nm at resolutions of 2 nm (700 nm), 8 nm (1400 nm), and 6 nm (2100 nm).

Field spectroradiometers can be handheld, mounted on fixed supports (e.g., towers), or installed on mobile platforms (e.g., tractor-mounted systems). Their instantaneous measurements depend on factors such as sky conditions, illumination–instrument viewing geometry, instrument settings, field techniques, measurement methods, and the parameter of interest (e.g., radiance or reflectance). Field spectroscopy protocols aim to minimize ambient scattered light and human interference on measured surfaces, while standardized data processing ensures reproducible, comparable results for calibration and reference (Figure 3). Field spectroscopy must account for the anisotropic angular distribution of solar irradiance and the variations in target reflectance due to viewing geometry (described by the bidirectional reflectance-distribution function, BRDF). Most field measurements collect radiance at a specific viewing angle and field of view, known as the hemispherical-conical reflectance factor (HCRF). Consequently, field methods, instruments, and data processing procedures are designed to convert these angular radiance measurements into hemispherical reflectance products using BRDF corrections.

Field spectroscopy also enables small-scale property estimation: for instance, reflectance spectra of plant leaves can be used to determine biochemical and biophysical traits. In addition, field spectroscopy is essential for calibrating airborne and satellite HRS sensors and supports the scaling of measurements from small areas (e.g., individual leaves) to broader scenes (e.g., vegetation canopies), and ultimately to image pixels.

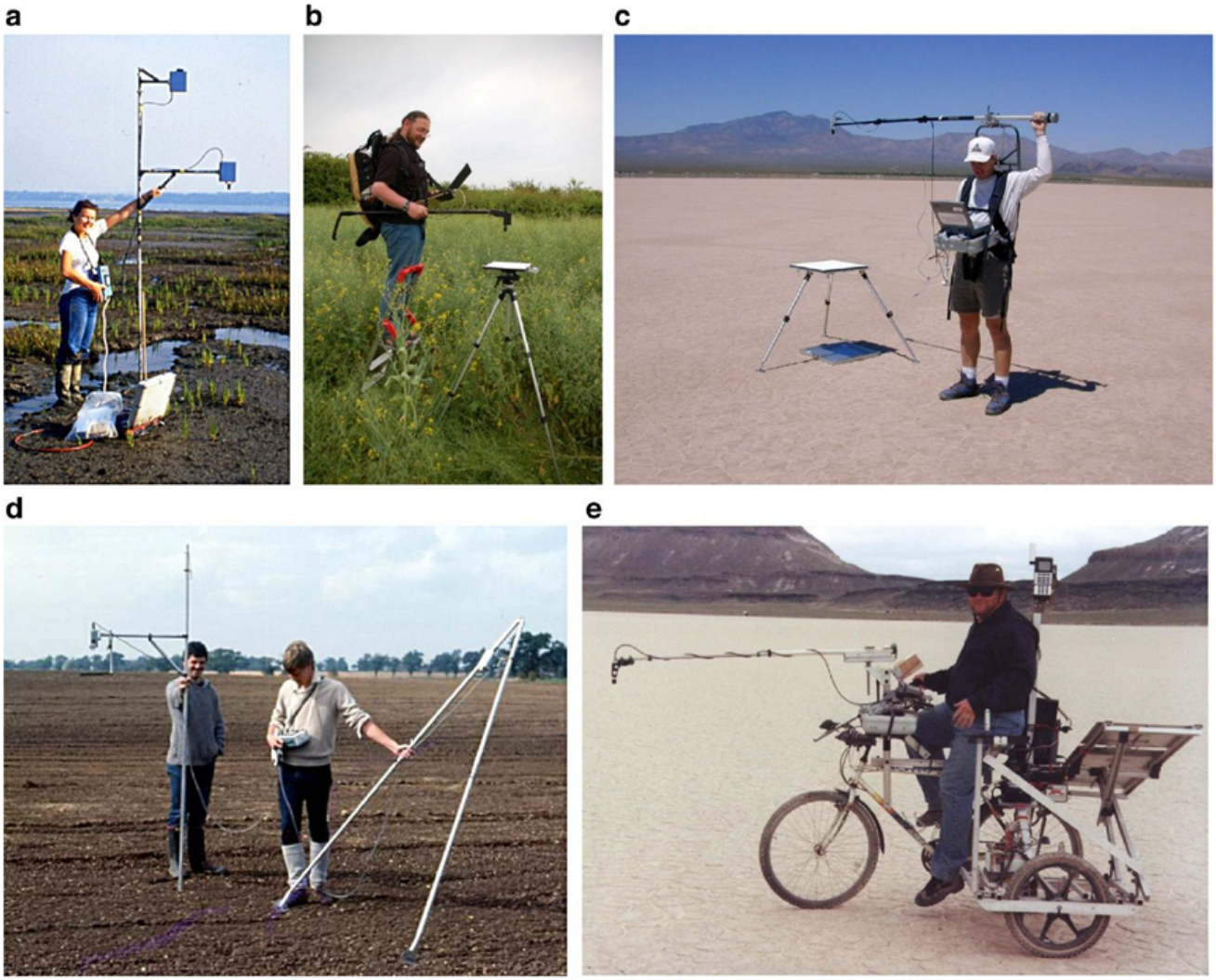

Figure 3. Variations on the ‘hand-held’ methodology. (a) a dual-beam Spectron SE590 being used from a lightweight mast to measure the reflectance of intertidal vegetation, (b) measuring a Spectralon reference panel in a field of oil-seed rape, and (c), the same procedure at a vicarious calibration site (source University of Arizona), (d) a dual-beam multiband radiometer being used with an A-frame mast to measure the off-nadir reflectance of a soil surface, and (e) the NASA JPL ‘Reflectomobile’ in use at Lunar Lake, Nevada. Source: Milton et al., 2009; used with permission; NASA JPL).

4. Imaging HRS: Imaging Spectroscopy

Imaging spectroscopy is an HRS technique that acquires large-scale airborne or spaceborne hyperspectral images of land surfaces or other targets. The instrument used for this purpose is known as an imaging spectrometer. NASA’s Jet Propulsion Laboratory (NASA/JPL) pioneered the development of the first airborne imaging spectrometer (AIS) in the 1970s. In 1984, NASA/JPL launched the Airborne Visible/Infrared Imaging Spectrometer (AVIRIS) program, which has been recognized as one of the most accurate and well-calibrated airborne imaging sensors (Thompson et al., 2017).

In 2009, NASA/JPL began developing the Next Generation Airborne Visible/Infrared Imaging Spectrometer (AVIRIS-NG), which became operational in 2013 (Figure 4). AVIRIS-NG covers wavelengths from 380 to 2510 nm with a 5 nm sampling interval and has been deployed on multiple airborne platforms, including the Twin Otter aircraft (flight altitudes of 600–3000 m

with 1–4 m spatial resolution) and the ER-2 high-altitude research plane (flight altitude of 20,000 m with 17–20 m spatial resolution). A third instrument (AVIRIS-3) is currently under development at NASA/JPL and will measure wavelengths from 380 to 2500 nm with a 7.4 nm sampling interval.

Over the past few decades, additional airborne imaging spectrometers have been developed by various manufacturers, including the Compact Airborne Spectrographic Imager (CASI) by ITRES Research Ltd. (Alberta, Canada), as well as systems from Headwall, Specim, and HySpex.

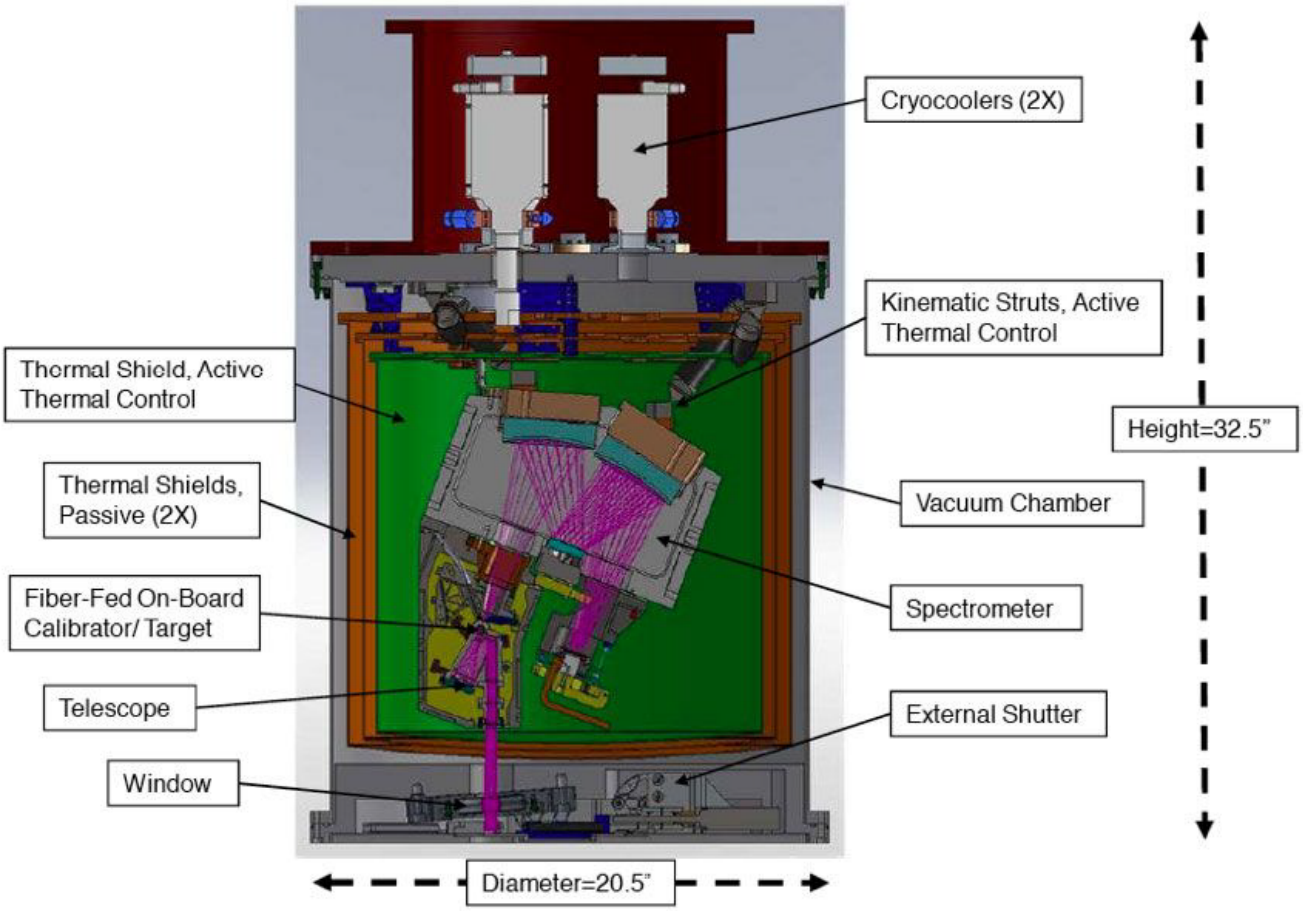

Figure 4. CAD model of the AVIRIS-NG sensor. Source: NASA JPL.

Spaceborne imaging spectrometer development began in the early 1980s. In November 2000, NASA launched Hyperion aboard the Earth Observing-1 (EO-1) satellite, widely recognized as the first spaceborne imaging spectrometer. Hyperion is a pushbroom instrument that acquires images 7.65 km across track and 185 km along track, encompassing 242 spectral bands (400–2500 nm) with a spatial resolution of 30 m. After Hyperion was decommissioned in 2007, NASA and other international space agencies introduced new spaceborne imaging spectrometers. Table 1 summarizes these instruments and their key characteristics.

Table 1. A list of past, current, and planned spaceborne hyperspectral imaging

spectrometers. Landsat-Next is included in this table as its broad coverage from visible to short-wave infrared wavelengths. Adapted from Ustin and Middleton, 2024.

Satellite / Instrument	Launch Date	Orbit Type	Altitude/Swath km	Temporal Resolution	Equatorial Crossing Time	UV/VNIR/SWIR, 380-2500 nm, GSD in m
NMP/Hyperion/EO-1	2001-2007	polar, LEO, sun synchronous	691/7.7	annually	9:45D	357–1000, 900–1600 nm @10 nm/band = 120 bands @ 0 m GSD, 1600–2576 nm@ 10 nm/band= 95 bands @30 m GSD
Italian Space Agency (ASI) PRecursore IperSpettraie della Missione Applicativa (PRISMA)	2019-2025	polar, LEO, sun-synchronous	615/30	29d	10:30D	66 bands, 400–1010 nm at 10 nm bandwidth@ 30 m GSD, 171 bands, 920–2505 nm at 10 nm bandwidth @ 30 m GSD
German Space Agency (DLR) Environmental Monitoring and Analysis Program (EnMAP)	2022–2026	polar, LEO, sun-synchronous	653/30	27d	11:00D	92 bands, 420–1000 nm; 6.5 nm ave. bandwidth @30 m GSD, 48 bands SWIR 1:900–1380 nm; 28 bands SWIR 2: 1480–1760 nm; 50 bands SWIR3: 1950–2450 nm, 10 nm ave. bandwidth @30 m GSD
DLR Earth Sensing Imaging Spectrometer (DESIS)	2017-2024	51.6◦ drifting orbit (on international space station)	407/30	3 d spatial repeat, but 63d for time of day repeat (TOD)		240 VNIR (450–915 nm) with ~1.9 nm bandwidths, @ 30 m GSD
HISUI Hyperspectral imager and Multispectral imager; Japanese Ministry of Education, Culture, Sports, Science and Technology (MEXT) and Japanese Space Agency (JAXA)	2019-2024	51.6◦ drifting orbit (on international space station)	407/20	3 d spatial repeat, but 63d for TOD		185 bands 400–250 nm, with 10.0–12.5 nm spectral resolution, IFOV is 20 m × 30 m
Earth Surface Mineral Dust Source Investigation (EMIT). NASA Earth Ventures Instrument (EVI-4)	2022-2026	51.6◦ drifting orbit (on international space station)	407/75	3 d spatial repeat, but 63d for TOD		286 bands 380–2500 nm at 7.4 nm sampling, @60 m GSD
PACE Ocean Color Instrument (OCI)	2024-2027	polar, LEO, sun-synchronous	676/2663 at 20◦ Tilt to avoid sungliht	1-2d	12:00D	46 bands from 342.5–887 nm at 5 nm resolution, 7 bands NIR-SWIR bands 940, 1038, 1250, 1378,1615, 2130, 2260 nm @ 1 km GSD.
Carbon Mapper Tanager satellites from Planet	first 2 Tanager satellites, 2024; Phase 2 expansion 2025; 5 yrs	polar, LEO sun-synchronous	405/18 km, measured in 1200 km wide-strips	TBD	TBD	Pushbroom VSWIR imaging spectrometer 300–2500 nm with 5 nm spectral sampling @30 m GSD
MethaneSat Environmental Defense Fund and New Zealand Space Agency	launched 3/4/2024, 5 yrs	51.6◦ Drifting Orbit	590/200	3-4 days global	TBD	VSWIR 2 HgCdTe detectors, #1 with 2 bands having 28 channels between 1249 1305 nm and 42 channels between 1598–1683nm w/0.2 nm resolution and 0.6nm spectral sampling @ 100 × 400 m GSD. SNR 190. #2 VSWIR HgCdTe detectors: 400 channels from 1583–1683 nm with 0.25 nm resolution and 0.08 nm sampling. @100 × 400 m GSD and SNR 190.
NASA Surface Biology and Geology (SBGVSWIR)	2029-2032	polar, LEO, sun synchronous	623/185	16d	11:00D	VNIR 52 bands 380–900, 10 nm sampling @ 30 m GSD, SWIR 1605 bands from 900–2500 nm @ 30 m GSD

Satellite / Instrument	Launch Date	Orbit Type	Altitude/Swath km	Temporal Resolution	Equatorial Crossing Time	UV/VNIR/SWIR, 380-2500 nm, GSD in m
Copernicus Sentinel Expansion Mission Copernicus Hyperspectral Imaging Mission for the Environment (CHIME), A, B	A 2029-2034, B 2031–2037	polar, sun-synchronous	786/290	25d, together 12.5 d	10:45D	~210 bands 400–2500 nm @ ≤10 nm; 20–30 m GSD band dependent
Landsat-Next (L-10), w/3 Platforms, LandIS instrument	2030-2038	polar, LEO, sun synchronous	653/164	16 (6 d w/3 together)	10:00	LandIS (bandwidth, nm) 5 bands: 490 (65), 560 (35), 665 (30), 842 (115), 1610 (90) nm, @ 12 m GSD, 10 bands 443 (20), 600 (30), 620 (20), 650 (35), 705 (15), 740 (15), 865 (20), 985 (20), 1035 (20), 1090 (20), 2038 (25), 2198 (20) @ 20 m GSD. Cal bands 412, 945, 1375 nm @ 60 m GSD

5. HRS Data Analysis

HRS data analysis encompasses a range of algorithmic techniques aimed at detecting, classifying, identifying, quantifying, and characterizing objects or features of interest in hyperspectral datasets. By leveraging the large number of narrow, contiguous spectral bands, researchers have adapted existing multispectral methods and developed specialized approaches that often yield superior performance. This section provides a concise overview of several common methods used in HRS data analysis.

5.1 Narrow-band Ratios

Band ratios derived from reflectance spectra have long been used to enhance spectral contrast and characterize objects. However, broad bandwidths in multispectral data can limit their ability to capture narrow absorption features. In contrast, HRS data offer hundreds of narrow bands, allowing for the development of narrow-band ratios that better isolate specific absorption features of target materials and biochemical constituents. For instance, narrow-band ratios in the 350–1,050 nm range outperform broad-band ratios in estimating agricultural crop biophysical traits (Thenkabail et al., 2000).

5.2 Spectral Unmixing Method

One persistent challenge in remote sensing is that a single pixel often encompasses multiple surfaces or materials, producing a composite spectrum that may not directly match the pure spectra of its constituent materials. Because HRS provides extensive spectral libraries of pure components, spectral mixture analysis (SMA) seeks to estimate the proportion of each material within the mixed pixel. A widely used and straightforward SMA approach assumes that the observed pixel spectrum is a linear combination of the pure substance (endmember) spectra, weighted by their fractional abundances. This linear unmixing technique has, for example, been employed to map specific vegetation species in the Santa Monica Mountains (Roberts et al., 1998).

5.3 Statistical Methods

The extensive number of bands in HRS data enables the quantification of physical and chemical properties (e.g., leaf pigments) via spectral measurements grounded in spectroscopic principles. These methods originated from laboratory-based research on

animal feed and forage quality, where statistical models were employed to link laboratory spectra with biochemical measurements under controlled conditions (Norris et al., 1976). Traditional statistical techniques, such as stepwise multiple linear regression (SMLR), can lead to overfitting when too many independent variables are used to predict a single dependent variable. Consequently, there has been a growing emphasis on methods that leverage the entire hyperspectral range, such as partial least squares regression (PLSR), rather than relying on a small subset of highly correlated bands, as is typical in SMLR (Qi et al., 2014).

5.4 Radiative Transfer Model

Another widely used approach to quantify physical and chemical properties using HRS data is the radiative transfer model (RTM), a physically based framework for characterizing how light interacts with matter. For instance, the PROSPECT model simulates leaf directional hemispherical reflectance and transmittance based on biochemical constituents such as chlorophyll, water, and dry matter (Jacquemoud & Baret, 1990). The SAIL model extends this concept to canopy reflectance by accounting for leaf area index, leaf angle distribution, and leaf size throughout multiple leaf layers (Verhoef, 1984). The SCOPE model further incorporates the transfer of incident light along with thermal and fluorescence emissions, component temperatures, photosynthesis, and turbulent heat exchange (Van der Tol et al., 2009).

Inversion of an RTM involves identifying the vegetation parameters that reproduce observed reflectance spectra. However, this inversion is often ill-posed: different parameter sets may yield similar modeled spectra, and measurement uncertainties combined with RTM assumptions can introduce inaccuracies. To mitigate these issues, various methods—such as look-up tables, neural networks, and the incorporation of prior information—have been developed to guide the inversion process.

5.5 Image Classification and Object Detection

Image classification and object detection are longstanding tasks in remote sensing. Machine learning (ML) and deep learning (DL) techniques have become especially powerful for analyzing HRS data, owing to their ability to handle high-dimensional inputs and complex spectral features—often surpassing traditional statistical methods designed for multispectral data. For instance, machine learning algorithms such as Support Vector Machines (SVM), Random Forests, k-Nearest Neighbors (k-NN), and gradient boosting, as well as deep learning architectures like Convolutional Neural Networks and the Segment Anything Model, have been employed to extract spatial and spectral features in HRS imagery for classification and object detection (Paoletti et al., 2019).

6. HRS Applications

HRS can support a broad range of remote sensing applications, such as soil property characterization (Ben-Dor et al., 2009), freshwater ecosystem biophysical assessments (Hestir et al., 2015), and snow property analysis (Dozier et al., 2009). By leveraging its high spectral resolution, HRS enables more precise identification of materials and quantitative determination of their physical and chemical properties through specialized analytical methods. HRS is particularly valuable in scenarios where multispectral techniques prove insufficient or cannot capture the level of detail required. This section provides a brief overview of a vegetation trait case study to illustrate both the advantages and challenges

of HRS.

Vegetation physiology and ecology are prominent application areas for HRS, where reflectance spectra have facilitated the quantification of numerous traits and functions, such as leaf area index (LAI), absorbed photosynthetically active radiation (fPAR), canopy temperature, leaf water, chlorophyll, ancillary pigments, cellulose, and lignin (Ustin et al., 2009). Most existing studies, however, are region-specific and rely on limited field or airborne HRS observations. A recent large-scale evaluation (Wang et al., 2023) assessed both physically based (RTM inversion) and empirically based approaches to trait prediction using two extensive HRS datasets (totaling 3,861 foliar samples) from 24 field sites across the eastern United States and southern China.

The results showed that both RTM inversion (using PROSPECT and PROCOSINE) and empirical models (partial least squares regression) accurately estimated vegetation traits. However, while RTM inversion strategies exhibited strong transferability across different datasets, empirical models yielded poorer performance when applied to independent datasets. This finding highlights the importance of generalized trait models, particularly regarding the calibration and refinement of leaf RTMs, as well as the integration of representative samples when training empirical models. Future efforts will focus on developing operational approaches for large-scale retrieval of vegetation and ecological variables using spaceborne HRS data.

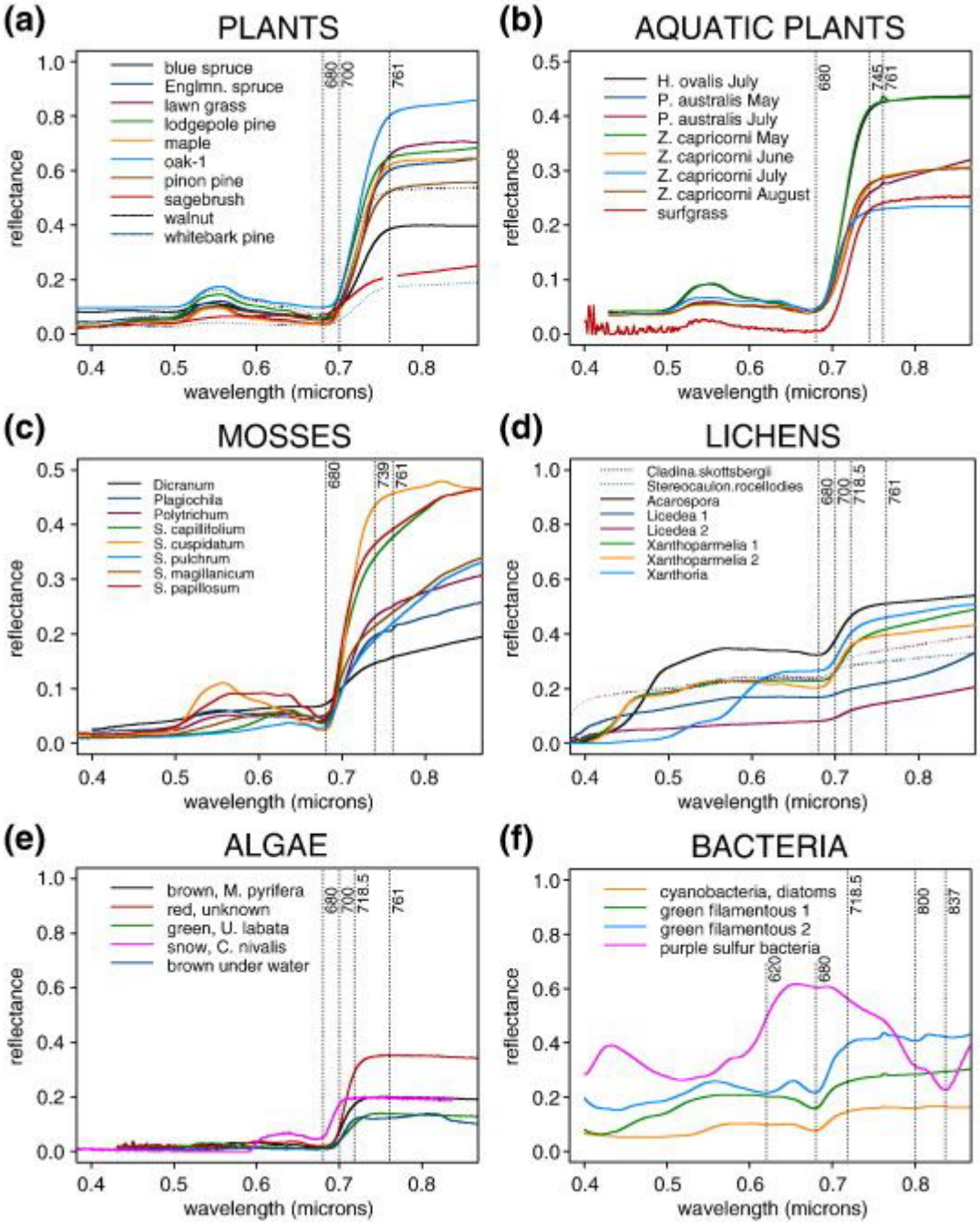

Figure 5. Characteristic reflectance patterns among major groups of photosynthetic organisms in the visible and near-infrared spectrum. The oxygen absorption band, included for reference, is the vertical bar at 761 nm on the near-infrared plateau, shorter wavelength bars indicate the primary chlorophyll band at 680 nm and the region of the red-edge inflection point. Source: Ustin et al., 2009; used with permission.

7. Future of HRS

The future of HRS is promising, with significant advancements expected in sensor technology, data processing, and applications across diverse fields. Many governmental agencies and private-sector entities worldwide have launched or planned HRS satellites for global-scale studies in the 2020s and 2030s (Table 1). The expansion of these satellites will provide essential, high-resolution spectral observations to advance research on biogeochemical processes, climate change, natural resources, and sustainable

development. Data fusion further strengthens HRS applications by integrating hyperspectral data with other remote sensing datasets at varying spectral and temporal resolutions, thus leveraging the strengths of multiple systems. For instance, Landsat and Sentinel imagery can fill temporal gaps in hyperspectral data from satellites such as PRISMA (Italy) and EnMAP (Germany), expanding coverage and enhancing time series analyses.

To address the growing volume of HRS data, machine learning (ML) and deep learning (DL) will be pivotal for automating data processing and analysis, thereby improving accuracy and efficiency in classification, object detection, anomaly detection, and feature extraction (Yuan et al., 2020). Moreover, new analytical tools and IT infrastructures—supported by cloud computing and artificial intelligence—are essential for enhancing the reproducibility, replicability, and reliability of HRS data analyses.

References

Ben-Dor, E., Chabrillat, S., Dematte, J. A. M., Taylor, G.R., Hill, J., Whiting, M.L., and Sommer, S. (2009). Using Imaging Spectroscopy to study soil properties. Remote sSensing of Environment, 113:S38–S55,

Curran, P.J. (1989). Remote sensing of foliar chemistry. Remote Sensing of Environment, 30, 271-278.

Dozier, J., Green, R. O., Nolin, A. W., & Painter, T. H. (2009). Interpretation of snow properties from imaging spectrometry. Remote Sensing of Environment, 113, S25-S37.

Goetz, A. F. H., Vane, G., Solomon, J., & Rock, B. N. (1985). Imaging Spectrometry for Earth Remote Sensing. Science, 228, 1147−1153.

Hestir, E. L., Brando, V. E., Bresciani, M., Giardino, C., Matta, E., Villa, P., & Dekker, A. G. (2015). Measuring freshwater aquatic ecosystems: The need for a hyperspectral global mapping satellite mission. Remote Sensing of Environment, 167, 181-195.

Jacquemoud, S. & Baret, F. (1990). PROSPECT: A model of leaf optical properties spectra. Remote Sensing of Environment, 34, 75−91.

Kokaly, R. F., Asner, G. P., Ollinger, S. V., Martin, M. E., & Wessman, C. A. (2009). Characterizing canopy biochemistry from imaging spectroscopy and its application to ecosystem studies. Remote Sensing of Environment, 113, S78-S91

Milton, E. J., Schaepman, M. E., Anderson, K., Kneubühler, M., & Fox, N. (2009). Progress in field spectroscopy. Remote Sensing of Environment, 113, S92-S109.

Norris, K. H., Barnes, R. F., Moore, J. E., & Shenk, J. S. (1976). Predicting Forage Quality by Infrared Reflectance Spectroscopy. Journal of Animal Science, 43, 889−897.

Paoletti, M. E., Haut, J. M., Plaza, J., & Plaza, A. (2019). Deep learning classifiers for hyperspectral imaging: A review. ISPRS Journal of Photogrammetry and Remote

Sensing, 158, 279-317.

Qi, Y., Dennison, P. E., Jolly, W. M., Kropp, R. C., & Brewer, S. C. (2014). Spectroscopic analysis of seasonal changes in live fuel moisture content and leaf dry mass. Remote Sensing of Environment, 150, 198-206.

Roberts, D. A., Gardner, M., Church, R., Ustin, S., Scheer, G., & Green, R. O. (1998). Mapping chaparral in the Santa Monica Mountains using multiple endmember spectral mixture models. Remote Sensing of Environment, 65(3), 267-279.

Thenkabail, P. S., Smith, R. B., & De Pauw, E. (2000). Hyperspectral Vegetation Indices and Their Relationships with Agricultural Crop Characteristics. Remote Sensing of Environment, 71(2), 158-182.

Ustin, S. L., & Middleton, E. M. (2024). Current and Near-Term Earth-Observing Environmental Satellites, Their Missions, Characteristics, Instruments, and Applications. Sensors, 24(11), 3488.

Ustin, S. L., Gitelson, A. A., Jacquemoud, S., Schaepman, M., Asner, G. P., Gamon, J. A., & Zarco-Tejada, P. (2009). Retrieval of foliar information about plant pigment systems from high resolution spectroscopy. Remote Sensing of Environment, 113, S67-S77.

Van der Tol, C., Verhoef, W., Timmermans, J., Verhoef, A., & Su, Z. (2009). An integrated model of soil-canopy spectral radiances, photosynthesis, fluorescence, temperature and energy balance. Biogeosciences, 6(12), 3109-3129.

Verhoef, W. (1984). Light scattering by leaf layers with application to canopy reflectance modeling: the SAIL model. Remote Sensing of Environment, 16, 125−141.

Wang, Z., Féret, J. B., Liu, N., Sun, Z., Yang, L., Geng, S., ... & Townsend, P. A. (2023). Generality of leaf spectroscopic models for predicting key foliar functional traits across continents: A comparison between physically-and empirically-based approaches. Remote Sensing of Environment, 293, 113614.

Yuan, Q., Shen, H., Li, T., Li, Z., Li, S., Jiang, Y., Xu., H., Tan, W., Yang, Q., Want, J., Gao, J. and Zhang, L. (2020). Deep learning in environmental remote sensing: Achievements and challenges. Remote sensing of Environment, 241, 111716.